Cancer Research

A Novel Mouse Model to Study Image-Guided, Radiation-Induced Intestinal Injury and Preclinical Screening of Radioprotectors

Ioannis I. Verginadis[1], Rahul Kanade[1], Brett Bell[1], Sravya Koduri[2], Edgar Ben-Josef[1], and Constantinos Koumenis[1]

Abstract

Radiation is an important treatment modality for gastrointestinal tumors, but intestinal injury is a common side effect. Here we describe a physiologically relevant model for studying the molecular determinants of radiation-induced intestinal damage and testing novel radioprotectors. The model employs a radiopaque marker implanted into the surface of the mouse jejunum, serving as a fiducial marker for precise radiation targeting. Mice were imaged with Cone-Beam CT (CBCT) and irradiated (IR) to the marked area using the Small Animal Radiation Research Platform (SARRP). IR-induced damage was acute but reversible and largely restricted to the area of the marker, leaving the surrounding tissues intact. Although whole gut irradiation with these doses caused lethal GI syndrome, focal (5 mm) radiation of the intestine did not cause any weight loss or lethality. However, fibrosis and collagen deposition 4 months post-IR indicated chronic intestinal damage. A separate cohort of mice was treated daily with curcumin, a clinically tested radioprotector, prior to and post-IR. Curcumin-treated mice showed significant decreases in both local and systemic inflammatory cytokine levels and in fibrosis, suggesting it is an effective radioprotector of the intestine. Our results indicate that this model, which emulates clinically relevant intestinal radiation-induced injury, can be used to assess radioprotectors prior to testing in the clinic. *Cancer Res; 77(4); 908–17. ©2016 AACR.*

Introduction

Radiotherapy is an important modality in cancer treatment with approximately half of all cancer patients receiving radiotherapy during the course of their treatment (1). As many patients receiving radiotherapy for abdominal or pelvic malignancies experience some form of radiation-induced gastrointestinal injury, there is great interest in understanding the mechanisms behind this pathology and developing effective treatments for it (2). In addition, there is increased concern regarding intentional or accidental exposure of humans to large doses of ionizing radiation due to the onset of acute radiation syndrome (ARS). ARS is comprised of three phases: the hematopoietic phase, gastrointestinal phase, and neurovascular phase in a dose-dependent order (3). Therapies currently exist to manage the hematopoietic phase, although no significant countermeasures exist to address the gastrointestinal or neurovascular phases at this time.

At present, animal models for targeted irradiation (IR) of the small intestine, which mimic clinical patient care, are scarce. This is due to the fact that the prevailing models require either whole body or abdominal irradiation, or require a surgical exteriorization of the small intestine. A more physiologically relevant model, which does not require repeated surgeries, was developed by Hauer-Jensen and colleagues involving transposition of a loop of the ileum to the animal's scrotum, allowing local irradiation of that segment (4). However, this model may only be used on segments of the gastrointestinal tract in close proximity to the scrotum. The model described in this article allows for targeted *in situ* irradiation of small intestinal segments. Moreover, the model only requires a single, minimally invasive surgery, which is used to place radiopaque markers for image-guided radiation. In addition, multiple fractions of conformally delivered irradiation may be administered without additional surgical intervention. This model is essential for understanding the pathophysiology of radiation injury, and testing potential novel radioprotectors and mitigators to improve cancer radiotherapy and be able to respond to radiologic incidents.

One potential radioprotective agent for the small intestine is curcumin, the principal curcuminoid of turmeric (*Curcuma longa*). Curcumin has a long history of use in traditional medicine. It is known to have oxygen radical–scavenging abilities as well as anti-inflammatory actions during a damage response (5). We and other groups have shown that it acts as a radiosensitizer in cancerous tissue while acting as a radioprotector in normal tissue (5, 6). Furthermore, it has a low toxicity profile with humans being able to tolerate at least 12 g per day of oral curcumin (7). Although curcumin exhibits low bioavailability in plasma, it shows the highest concentration in the gastrointestinal tract after oral gavage treatment (8). Along these lines, curcumin has been shown to be a radioprotector in the ileum when administered orally (9, 10). Therefore, we tested the ability of curcumin to

[1]Department of Radiation Oncology, The Perelman School of Medicine, University of Pennsylvania, Philadelphia, Pennsylvania. [2]Department of Biology, Drexel University, Philadelphia, Pennsylvania.

Note: Supplementary data for this article are available at Cancer Research Online (http://cancerres.aacrjournals.org/).

Corresponding Author: Constantinos Koumenis, University of Pennsylvania School of Medicine, SCTR Bldg Room 8-087, 3400 Civic Center Blvd, Philadelphia, PA 19104-5156. Phone: 215-898-0076; Fax: 215-898-0090; E-mail: costas.koumenis@uphs.upenn.edu

doi: 10.1158/0008-5472.CAN-16-2724

protect against cellular and tissue-level changes associated with fibrosis, a clinically relevant outcome in radiotherapy of the GI tract.

Our model allows for image-guided, targeted *in situ* irradiation of short intestinal segments. It constitutes a new tool to rapidly evaluate multiple biological markers of DNA damage in the mouse intestine and we believe it will be valuable in future screens for radiation response modifiers and the study of molecular aspects of IR damage.

Materials and Methods

Mice

Eight to 10-week-old female C57BL/6 mice (The Jackson Laboratory) were maintained in the University of Pennsylvania animal facilities. All experimental procedures were conducted in accordance with the guidelines and protocols approved by the Institutional Animal Care and Use Committee. Mice were subjected to image-guided radiation using the Small-Animal Radiation Research Platform (SARRP) and euthanized to collect small intestine segments for immunofluorescence and histology staining. A cohort of animals received 100 mg/kg of curcumin (Sigma Aldrich, C1386) three days before irradiation and 2 months after irradiation via oral gavage. All mice were injected intraperitoneally (i.p.) with 200–400 μg of 5-ethynyl-2′-deoxyuridine (EdU; Thermo Fisher Scientific C10337) in PBS 3–4 hours before euthanasia. Three or more mice were used in each group. More details are found in Supplementary Material.

Implantation of the radiopaque marker

Animals were anesthetized using inhaled isoflurane at a concentration of 2%–2.5%. A 1–2 cm midline abdominal incision was made and the jejunum of the mouse was exposed *in situ*. One side of the radiopaque marker was coated in Medbond Tissue Glue and then rapidly applied to the middle of the jejunum. The peritoneum was sutured using 5-0 PGA-PCL absorbable sutures (McKesson) and the skin was sutured using 5-0 Nylon nonabsorbable sutures (Ethicon). All surgical procedures were conducted aseptically. Mice were administered with 10 mg/kg of meloxicam subcutaneously every 24 hours for 72 hours and with 1 mg/kg of sustained-release buprenorphine at the time of surgery. Animal weights and survival were monitored from the time of surgery until euthanasia.

Cone-Beam CT imaging and radiation

For these studies, all mice were imaged and irradiated while immobilized with 2.5% isoflurane anesthesia with medical air as the carrier gas (VetEquip). Following 5 minutes in an induction chamber, the fully anesthetized mouse was placed on a customized platform in the ventral recumbent position. The head of the mouse is placed in a face mask that allows the gas to be scavenged (Xerotec Inc.). The platform was placed off the stage of the SARRP (Xstrahl Life Sciences). Using the SARRP Control Interface, a Cone-Beam CT (CBCT) image was initiated with the X-ray tube operating at 65 kV, 0.5 mA with aluminum filtration. The images were reconstructed with Xstrahl's MuriSlice Software. Dosimetry was performed by measuring EBT2 gafchromic film exposure, at depth using solid-water phantom material, with a Microtek Artixcam M1 camera. The dose-exposure calibration was done using a cesium irradiator with calibration dose rate. Utilizing the software, the surgically implanted radiopaque marker was visualized and an isocenter was selected for targeted radiotherapy (Supplementary Fig. S1A). Once the isocenter was determined, the robotic stage moved the animal to the proper location. Final adjustments of the beam delivery angle to avoid the spine were made if necessary. Delivery of the 12 or 18 Gy single dose was made using a 5×5 mm collimated beam operating at 175 kV, 15 mA with copper filtration (Supplementary Fig. S1A). The dose rate was 1.65 Gy/minute. All imaging and X-ray irradiations in this study were approved and in compliance with the Institutional Animal Care and Use Committee (IACUC) at the University of Pennsylvania (Philadelphia, PA).

Immunofluorescence, EdU, γH2AX, and TUNEL staining, crypt microcolony assay

Samples were processed and stained as described previously (11–13). Details are given in Supplementary Material.

Cytokine/chemokine quantification

Intestinal tissue homogenates and plasma samples were analyzed for cytokine/chemokine levels as described previously (14). Details are given in Supplementary Material.

Plasma collection

Whole blood was collected into heparinized collecting tubes (Fisher Scientific, 02-668-10) also containing EDTA, from the tail vein of the mice pre- and 4 days postirradiation. Plasma was obtained by centrifugation for 10 minutes at 1,000–2,000 $\times$ *g* using a refrigerated centrifuge. Plasma samples were aliquoted and stored at −80°C.

Statistical analysis

Statistical analysis was carried out using GraphPad Prism V software. Data were presented as means ± SEM. Statistical significance was calculated with unpaired Student *t* test. $P < 0.05$ was considered to be significant.

Results

Radiopaque marker as a tool for radiation-induced localized intestinal damage

In the current study, we aimed to develop a mouse model that would be more pathophysiologically relevant to the intestinal injury sustained during a clinical course of radiotherapy to the abdomen. Unlike current animal models that mostly irradiate the whole abdomen, in clinical practice, patients receive high radiation doses to relatively small volumes of bowel and the radiation injury is focal. One week after the implantation of radiopaque markers, mice were placed under isoflurane anesthesia for CBCT scan and then irradiated with a single dose of 12 or 18 Gy using the SARRP (Fig. 1A). The implantation of the radiopaque marker on the jejunum of the C57BL/6 mice was well tolerated. Of 120 mice that were used in this study, 5 mice (4.2%) died because of intestinal infection and sepsis, while 12 (10%) died of jejunum obstruction. No mortality was associated with anesthesia (mice were generally awoke 2–3 minutes after the isoflurane was removed). To minimize mortality, a small, 1-cm incision in the abdominal area was made followed by suturing both the peritoneum (with absorbable sutures) and epidermis (regular sutures; Fig. 1B). The whole procedure took place under an aseptic environment.

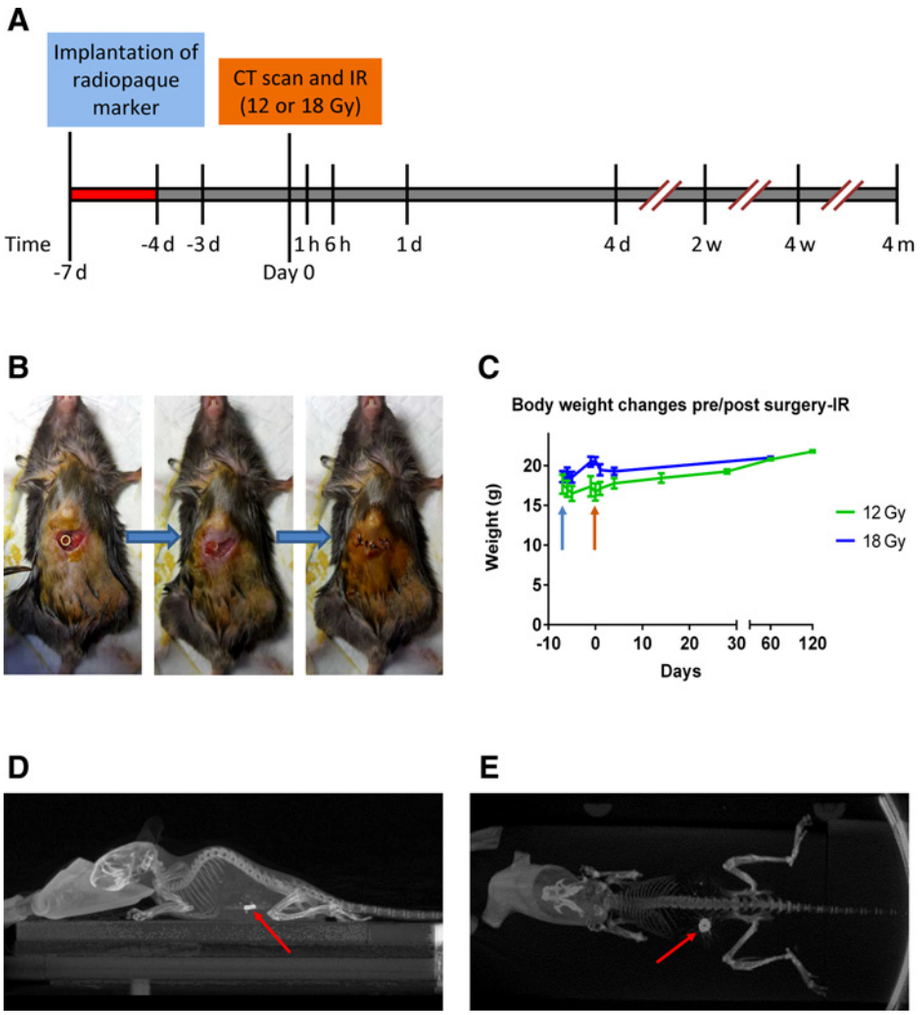

Figure 1.
Implantation of the radiopaque marker and tracking by CT scan. **A,** Schematic presentation of the experimental design. Red area indicates the treatment period with analgesics and anti-inflammatory drugs post-surgery. Mice were euthanized for intestinal tissue collection at various time points post-radiotherapy (RT) as indicated; h, hours; d, days; w, weeks, m, months. **B,** Implantation of radiopaque marker on the jejunum of the C57BL/6 mice starting with a small incision on the abdominal area (around 1 cm). Radiopaque marker was surgically glued and sutured to the peritoneum and epidermis with absorbable and regular sutures, respectively. **C,** Body weight changes postsurgery and pre/postradiation with a single dose of 12 and 18 Gy. Blue arrow, the time of radiopaque marker implantation; orange arrow, the time of radiation. Lateral (**D**) and dorsal view (**E**) of cone-beam CT of an anesthetized mouse scanned in the prone position.

Postoperation, the mice lost 2%–9% of their initial body weight, but their weights fully recovered by the time of the CBCT scan/IR (Fig. 1C), 7 days later. Moreover, there was a minor weight loss of the irradiated mice, which did not differ significantly from the unirradiated mice. A few days after irradiation, the mice resumed normal growth (Fig. 1C).

To locate the radiopaque marker for targeted radiotherapy, a CBCT image was obtained using the XStrahl's MuiriSlice Software and reconstructing the images and visualizing the marker on the mouse intestine (Fig. 1D and E; Supplementary Video S1). On the basis of the determined 3D location of the radiopaque marker, we are able to deliver the beam, with its angle adjusted to avoid the spine in the irradiated field (Supplementary Fig. S1B and S1C). The radiopaque marker was shown to be well tolerated by the mice without causing side effects that can impact their survival. For evaluation of the intestinal damage caused by radiation, mice were euthanized at various time points (Fig. 1A) and intestinal segments of 1.5 cm were harvested with the marker located in the middle of the tissue (Supplementary Fig. S2A and S2B). Then, the marker was removed and the intestine segment was placed in either optimal cutting temperature (OCT) medium or formalin for further processing (Supplementary Fig. S2B).

Intestinal cellular damage is restricted to the site of irradiation

The main objective of this is study was to test whether we could induce localized intestinal damage by radiation. We used several molecular methods to assay direct DNA damage or the biological consequences of DNA damage (e.g., inhibition of proliferation, apoptosis). One of the early subcellular effects after exposure to radiation is the phosphorylation of histone H2AX at serine 139 (γH2AX). Its detection is considered a sensitive and quantitative method for DNA double-strand breaks. Results from the immunofluorescence staining for γH2AX of the frozen tissues harvested at 1 hour post-IR, showed that the DNA damage was localized primarily at the site of the implanted marker (Fig. 2A). The size of the damaged area was 5–6 mm, consistent with the size of the collimator used in this study (5 × 5 mm; Fig. 2A and Supplementary Fig. S3A). It is noteworthy that there was no visible DNA damage on either side of the irradiated area (IR area) and that the γ-H2AX intensity decreased abruptly from the irradiated to the nonirradiated area (Supplementary Fig. S3B and S3C). The late-phase γH2AX foci (≥12 hours) are indicative of chromatin remodeling associated with unrepaired DSBs. To follow temporally the damage of the irradiated area, we performed a time-dependent analysis of the H2AX phosphorylation up to 24 hours post-IR. We found that the intensity of the γH2AX staining in all

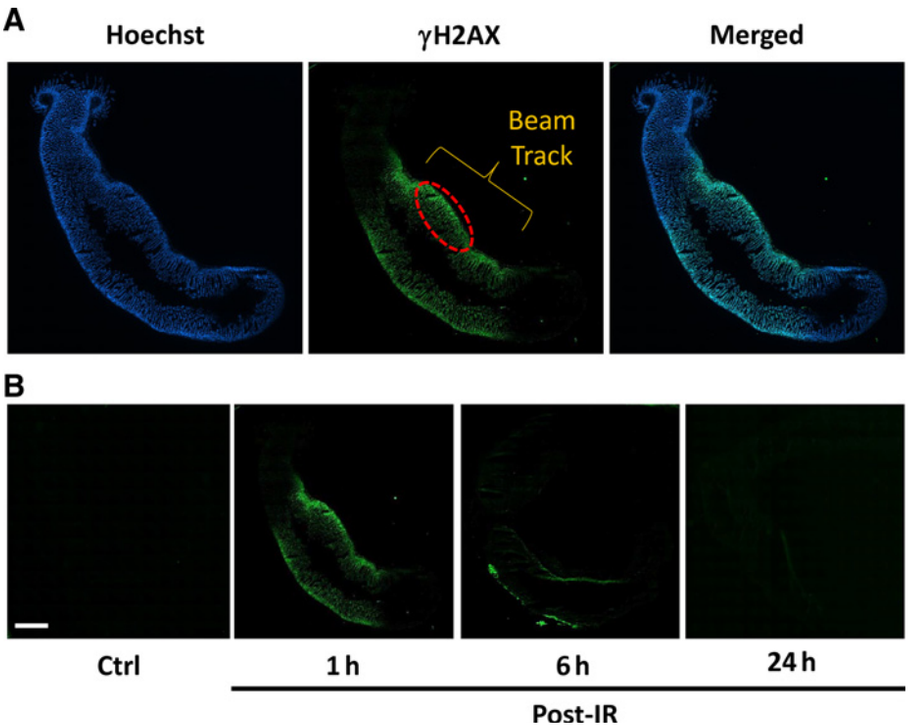

Figure 2.
Radiation-induced DNA damage at the site of the implanted marker. **A,** γH2AX immunofluorescence staining in OCT-frozen jejunum sections (magnification, ×10). Damage due to irradiation covers 5–6 mm of the intestinal tissue area, corresponding to the size of the collimator used (5 × 5 mm). The red dotted circle indicates the area of the implanted marker (middle of intestinal segment). **B,** γH2AX levels at different time points postirradiation compared with the control (magnification, ×10); scale bar, 1 mm.

compartments of the crypt-villus unit was gradually decreased by 6 hours post-IR, which coincides with dsDNA repair, while the signal was almost undetectable by 24 hours post-IR, indicating that there was no persistent DNA damage at the irradiated area at these high doses (Fig. 2B).

We also performed a time course analysis for EdU incorporation from 6 hours up to 4 weeks post-IR. The untreated tissue (control) showed a robust EdU incorporation (Fig. 3A and B). The intensity of the EdU immunofluorescence staining was significantly decreased in the irradiated tissues at 6 hours and 1 day post-IR (Fig. 3A). Representative images of single crypts show that the damaged area is characterized by fewer positive EdU cells as well as with lower intensity of the EdU immunofluorescence signal (Fig. 3B). On the basis of the staining at the latter time points, the induced damage can be characterized as acute because the proliferation of the crypt compartments was completely restored, starting from 4 days post-IR (Fig. 3A). This was also confirmed by the high number of the positive EdU cells per crypt as well as by the percentage of the regenerated crypts (Fig. 3C and D). Also, the damage was restricted mainly at the marker area without affecting the nonirradiated areas (Fig. 3E and F). Results from both γ-H2AX and EdU immunofluorescence staining indicate that the damage caused by radiation was highly restricted to the marker area without causing any significant damage to the surrounding tissues.

Radiation-induced acute damage is temporary and is characterized by increased apoptosis

Although radiation-induced damage can be repaired by DNA repair mechanisms, apoptosis can occur if the DNA damage above a certain threshold is unresolved. The extent of apoptosis as well as the type of cells damaged in the crypt dictates whether the damage is reversible or can lead to loss of cells and subsequently barrier function and death. Results from the immunofluorescence staining of the intestinal tissues using the TUNEL assay showed that the irradiated areas (on marker) presented a significant increase in apoptotic cells at 6 hours postradiation that remained high at 1-day time point, while apoptosis was barely detectable 4 days post-IR (Fig. 4A and B). This was presumably due to clearance of apoptotic bodies by immune infiltrating cells. Staining of the nonirradiated tissues revealed little, if any, apoptosis and no apparent loss of barrier function (Fig. 4C and D). These results are consistent with those from the EdU incorporation assay showing that radiation induced acute damage only at the marker site at early time points. This damage is temporary and the irradiated area fully recovered as characterized by the lack of apoptotic cells and the high levels of proliferative crypt compartments.

Strong inflammatory response at the acute phase and induction of fibrosis as a long-term effect after radiation

High doses of localized radiation can cause a permanent damage to the epithelial barrier and can lead to compromise of barrier function. In this process, there is activation of the immune system as well as induction of inflammatory responses accompanied by changes in the expression level of cytokines, chemokines, and transcription factors. To investigate the levels of inflammation following the two IR doses, we used a mouse-specific 11-plex cytokine microbead assay to assess the levels of inflammatory response at 4 days and 2 weeks postirradiation. We used whole tissue homogenates of the two different intestinal segments, on marker (OM) and distal to the marker (DM) from irradiated and mock-irradiated mice (Supplementary Fig. S4). The analysis of the OM tissue showed that the levels of 7 of 11 cytokines/chemokines were significantly induced at 4 days post-IR. Among them, IL6 and MIG/CXCL9 showed a 4.3- and

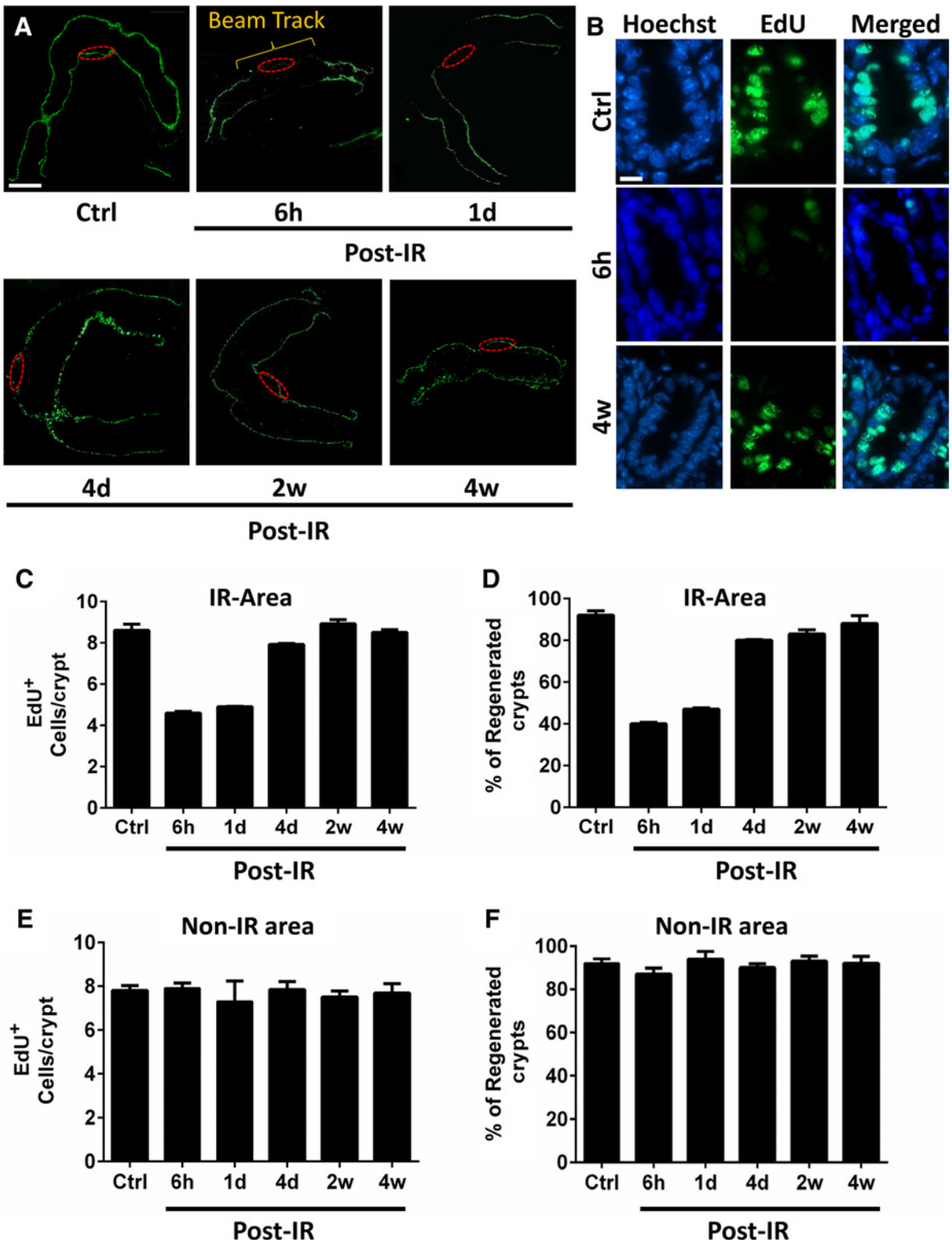

Figure 3.

Significant decrease of intestinal crypt cell proliferation after 12 Gy of radiation. **A,** EdU incorporation in control intestinal crypts or crypts irradiated with a single dose of 12 Gy. Tissues were harvested at the indicated time points postirradiation. Red circle, the site of implanted marker (magnification, ×10). **B,** Representative images of EdU immunofluorescence as in **A** at the indicated time points (magnification, ×63). **C** and **D,** Quantification of EdU-positive cells (**C**) and percentage of regenerated crypts in all time points post radiation as in **A** (**D**). **E** and **F,** Quantification of EdU-positive cells (**E**) and percentage of regenerated crypts per intestinal crypt of the non-IR area of mice treated with a single dose of 12 Gy (**F**). Values in **C–F** represent means ± SEM ($N = 3$); scale bar for **A** is 2 mm and for **B** is 20 μm.

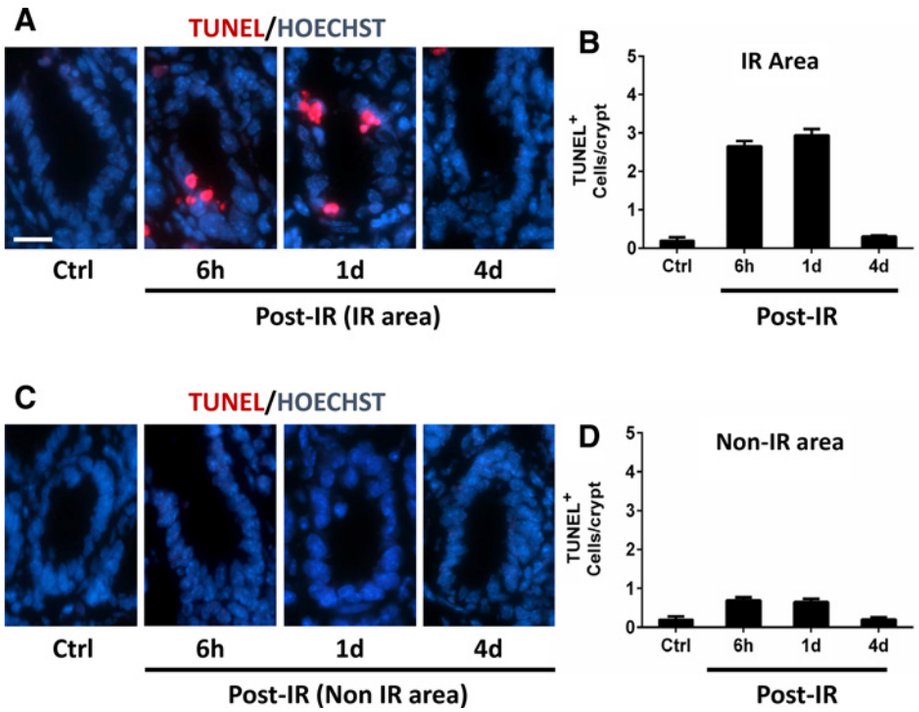

Figure 4.
Evaluation of apoptosis on intestinal crypts in response to 12 Gy. **A,** TUNEL immunofluorescence in the 12 Gy IR area—OM at the indicated time points (magnification, ×63). **B,** Quantification of TUNEL-positive cells in intestinal crypts of IR area, treated as in **A**. **C,** TUNEL immunofluorescence in the non-IR at the indicated time points (magnification, ×63). Quantification of TUNEL-positive cells in intestinal crypts of non-IR areas. Values in **B** and **D** represent means ± SEM ($n = 3$); scale bar, 20 μm.

2.7-fold increase ($P < 0.01$), respectively, followed by a 1.7- to 2-fold increase of the IL10 ($P < 0.05$), IL12 (p70; $P < 0.05$), and TNFα ($P < 0.01$; Fig. 5A). However, the levels of all cytokines subsided to pre-RT levels at 14 days post-IR. The cytokine/chemokine levels of the DM tissue showed that there was no significant inflammation on that area compared with that of the OM tissue at both time points (Fig. 5B).

It is known that late radiation damage in most of the normal tissues is characterized by the loss of parenchymal cells, collagen deposition and excessive formation of fibrous tissue (15–17). Thus, in addition to the acute effects of radiation on inflammatory response, we evaluated its long-term effects on the two intestinal segments at 4 months after 12-Gy irradiation. Our findings revealed focal ulcers with subtending submucosal and serosal fibrosis, crypt hyperplasia, as well as lymphocyte and plasma cell infiltration (Fig. 5C). The lesions were restricted to the marker site and the surrounding tissue was relatively spared, while the DM section was histopathologically similar as the nonirradiated tissue (Fig. 5D). These results demonstrate that both acute inflammatory responses as well as the delayed effects of radiation are restricted to the irradiated (marker site), without affecting the proximal and distal to marker tissues.

Significant reduction of IL6 levels and elimination of fibrosis by curcumin administration prior to and postradiation

We showed that focal radiation caused a significant elevation of proinflammatory and anti-inflammatory cytokines with most prominently induced cytokine at the irradiated area to be IL6. Collagen deposition and fibrosis are the characteristics of the delayed damage around the marker area 4 months postradiation. Curcumin has been found to possess antioxidant, anti-inflammatory, and antitumor activities in a variety of animal models of human diseases. Others and we previously showed that curcumin acts as a radiosensitizer in cancerous tissue while acting as a radioprotector in normal tissue. To check whether curcumin can confer radioprotection to the irradiated intestinal area in our model, mice were treated with 100 mg/kg of curcumin by oral gavage 3 days preirradiation and 2 months post-IR (Fig. 6A). Although, mice treated with curcumin did not present any difference in the EdU^+ cells/crypt (Fig. 6B), there was a significant decrease in the $TUNEL^+$ cells per crypt compared with the mice treated with vehicle (Fig. 6C). Results from the cytokine profile analysis (3-plex assay) on the intestinal lysates (OM only) 4 days post 18 Gy irradiation showed that IL6 levels increased a 6-fold while there was a 4.3-fold increase with 12 Gy. The levels of other tested cytokines were not significantly elevated. However, mice treated with curcumin and irradiation presented a significant decrease ($P < 0.05$) of the levels of IL6 with no significant variations in the levels of the other 2 cytokines compared with the irradiation-only cohort (Fig. 6D). In addition to the intestinal lysates, we also assessed the effects of curcumin at the systemic level. Blood plasma analysis showed that irradiation (18 Gy) caused an almost 4-fold increase on the IL6 levels at 4 days post-IR, which were significantly reduced after curcumin treatment ($P < 0.05$; Fig. 6E). It is noteworthy that curcumin treatment also decreased the basal levels of IL6, before IR.

Moreover, we also investigated the role of curcumin on the long-term effects post-IR. The single dose of 18 Gy caused a focal serosal fibrosis at the marker site (OM) compared with the tissue from mock-irradiated mice, as it is indicated by both H&E and Trichrome staining (Fig. 7A and B). Within the wall of this area, there was a focus of granulation tissue (proliferating fibroblasts along with neovascularization) and a mixture of inflammatory cells, lymphocytes, plasma cells and neutrophils. Sections from the mice treated with curcumin contained minimal multifocal areas of serosal fibrosis and there were few (mild) aggregates of lymphocytes, plasma cells, and neutrophils within the lamina propria throughout the section (Fig. 7A–C). These results indicate

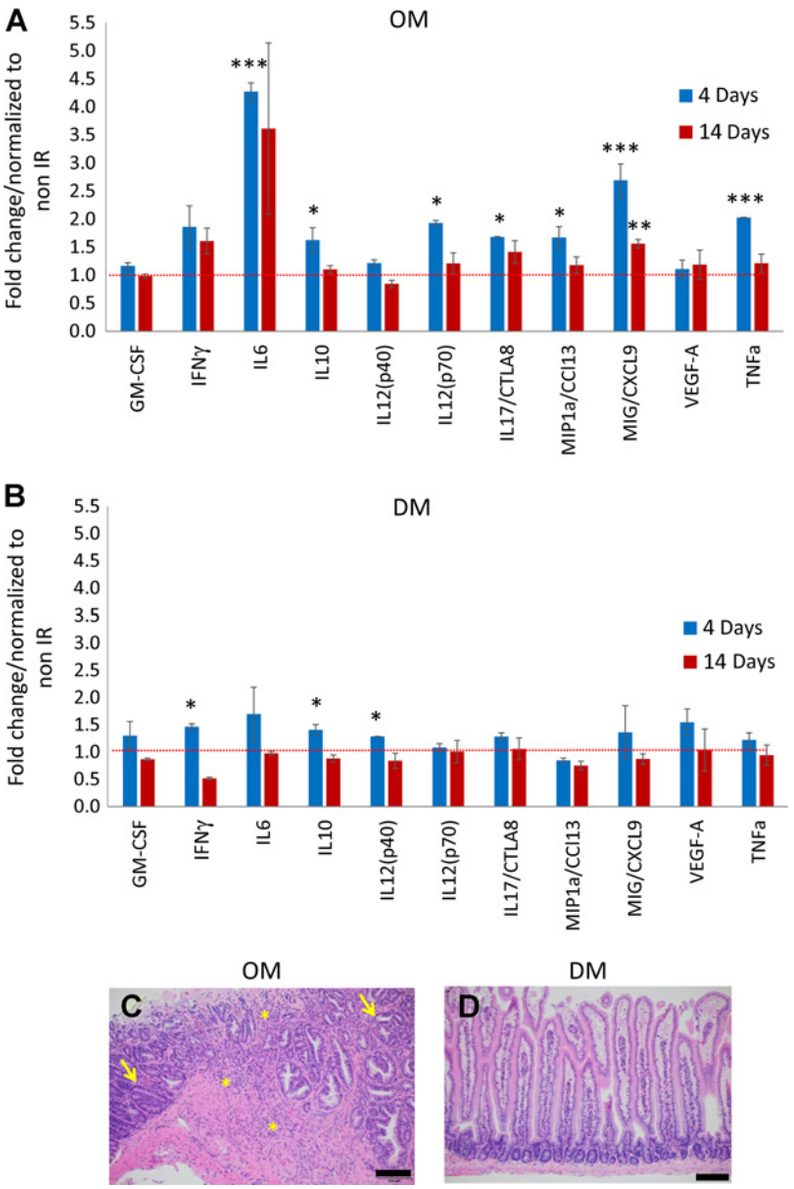

Figure 5.

Effects of focal irradiation on inflammatory mediators and chemokines in intestinal segment (1.5 cm) homogenates of the jejunum by a 11-plex cytokine analysis at 4 and 14 days post 12 Gy of radiation. Analysis was conducted on OM (**A**) and DM (**B**) segments. **C** and **D,** H&E staining of OM and DM segments, respectively, for detection of fibrosis at 4 months after 12 Gy of radiation (magnification, ×20). Arrows indicate the crypt hyperplasia, while the asterisks indicate the areas that characterized by high density of lymphocytes and plasma cell infiltration. Values represent means ± SEM ($n = 3$). Red dotted line, the basal levels of cytokines (control mice, no IR). Scale bar, 100 μm.
*, $P < 0.05$; **, $P < 0.01$; ***, $P < 0.001$.

that administration of curcumin significantly reduces the levels of inflammatory markers and substantially reduced the fibrosis formation as a long-term effect post-IR, suggesting it may be an effective radioprotector in the clinic.

Discussion

In the current study, we have developed and tested a novel mouse model of image-guided radiation-induced intestinal damage that can be used to assess the efficacy of novel radioprotectors. Using a radiopaque marker to guide the IR beam, we were able to cause focal intestinal damage similar to that encountered in the clinical practice of abdominal radiotherapy. We have also been able to demonstrate cytokine changes and molecular evidence of focal radiation injury in this model, as well as demonstrate a radioprotective effect of curcumin. Radiation-induced intestinal injury is the most important toxicity in clinical abdominal radiotherapy. In a review of 1,160 patients treated with hypofractionated radiotherapy for pancreatic cancer, serious gastrointestinal toxicities consisted of ulcers, hemorrhages, obstructions, structures, and perforations (18). The median late grade 3 or greater GI toxicity was 7.4% (but up to 32.7% in one report). The most frequently reported toxicity was non-hemorrhagic, nonperforated ulcer with a median rate of 9.1 % (range: 3.9%–20%). In another study of Stereotactic Body Radiotherapy (SBRT) for pancreatic cancer, the 12-month rate of G2 or higher GI toxicity was 29% (19). In patients who received 15 Gy or more to greater than 9.1 cm^3, the rate increased to 52%. Severe gastrointestinal toxicity was also the dose-limiting toxicity in a phase I/II clinical trial of fractionated chemoradiotherapy for unresectable pancreatic cancer (20).

This model builds upon other existing models of intestinal injury but offers several unique advantages. Prior models to study radiation-induced gastrointestinal injury involve an extensive

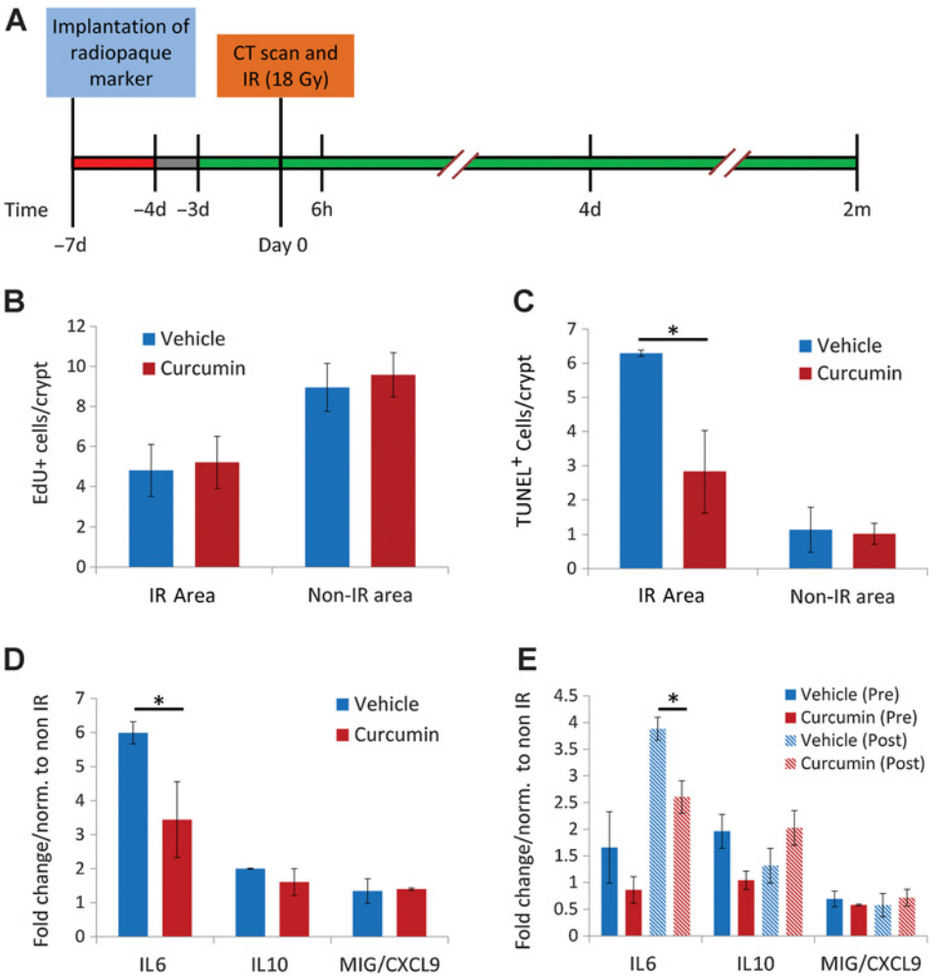

Figure 6.
Effects of 100 mg/kg of curcumin treatment (oral gavage) on acute (topically and systemically) effects after 18 Gy of focal radiation. **A,** Schematic presentation of the experimental design. Red and green areas indicate the treatment period with analgesics and anti-inflammatory drugs postsurgery and treatment with 100 mg/kg of curcumin, respectively. Mice were euthanized for intestinal tissue collection at various time points post-RT as indicated; h, hours; d, days; m, months. **B** and **C,** Quantification of EdU-positive cells (**B**) and TUNEL-positive cells (**C**) in intestinal crypts of mice treated with either vehicle or curcumin, 6 hours post 18 Gy of radiation. **D,** 3-plex cytokine analysis on intestinal lysates (OM segment) at 4 days post-radiation. **E,** Effects of curcumin on cytokine levels in plasma samples at 4 days after 18 Gy of radiation. Values represent means ± SEM ($n = 3$). *, $P < 0.05$.

surgical procedure to exteriorize a segment of the small intestine, placing the animal in a shielded container with only the exteriorized segment exposed, and irradiating the animal (4). While multiple surgical procedures may be conducted in dose fractionation studies with low mortality rates, this requires more resources and has a greater impact on the overall health of the animal when compared with single surgical procedures (21). Another method immobilizes a segment of the small intestine in a sleeve of abdominal muscle. One may then insert temporary sutures and apply tension to these sutures to pull the abdominal wall and attached jejunum through an opening in a lead box, which the animal is shielded in to allow for irradiation targeted to this segment (22). In addition, DeBoth and colleagues developed a rat model involving a Thiry-Vella fistula with both stomas placed in the scrotum (23). While the fistula formation preserves the vascular and mesenteric connections, the isolated loop no longer contains normal intestinal contents, which reduces the physiologic relevance of the model. A more physiologically relevant model that does not require repeated surgeries was developed by Hauer-Jensen and colleagues involving transposition of a loop of the ileum to the rat's scrotum, allowing local irradiation of that segment (4). However, this model may only be used on segments of the gastrointestinal tract in close proximity to the scrotum. In addition, only relatively small lengths of intestine may be translocated to the scrotum. Another limitation of rat models compared with the mouse models is that the latter can be genetically modified to study the molecular mechanisms of radiation-induced damage. Finally, the lower cost of using mouse models, renders them a more feasible model for this type of studies.

The model described in this article allows for targeted *in situ* irradiation of small intestinal segments utilizing the capabilities of the SARRP. The model only requires a single short surgery, characterized by low mortality rates, which may be used to place multiple markers. Although not tested in this study, our model also allows for multiple fractions of irradiation administered without additional surgical intervention, rendering it a more physiologically relevant mouse model of intestinal injury. The mechanism of acute intestinal injury involves the barrier of the intestinal epithelium becoming disrupted following ionizing radiation exposure. This is mainly attributed to apoptosis of the intestinal stem cells, being unable to repopulate the epithelium (24). Furthermore, late effects of radiation exposure to the bowel include an upregulation of cytokines (25) in the submucosa and the induction of fibrosis in the connective tissue (26).

Another important feature of the model we report herein is the ability to study radiation volume effects. In clinical radiotherapy, it has been appreciated for a long time that intestinal toxicity is influenced not just by the maximal dose delivered to

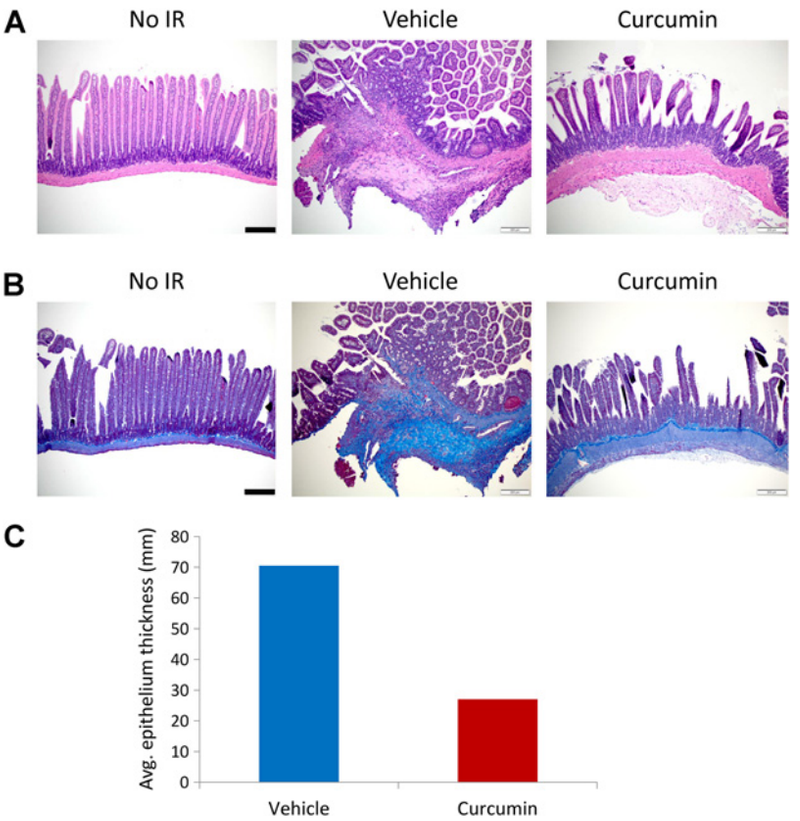

Figure 7.
Effects of 100 mg/kg of curcumin treatment (oral gavage) on chronic effects after 18 Gy of focal radiation. H&E staining (**A**) and Trichrome staining of OM segments (**B**) from mice treated with either vehicle or curcumin, 2 months post 18 Gy of radiation or mock-irradiated mice (magnification, ×20). **C,** Quantification of fibrosis from **B**. Values represent means ($n = 2$). Scale bar, 200 μm.

the intestine, but by the volume of intestine irradiated as well (27). However, the exact relationship between dose and volume of irradiated intestine and toxicity, and the mechanisms underpinning this observation remain mostly unknown. We believe our model will be very useful in elucidating these details, which, in turn, would be a very significant contribution to the clinical care of cancer patients. It is interesting to note in this context that in our model, we do not see any mortality when we induce a focal intestinal injury with high radiation doses (i.e., up to 24 Gy). This is very different that the mortality observed after whole abdominal radiation to much lower doses (typically LD50s are around 14 Gy).

Although radiosensitization is important to enhance tumor control, equally important is normal tissue toxicity minimization. Clinically approved radioprotectants are currently limited, with amifostine being the most potent and widely used clinical agent for head and neck cancer by scavenging the free radicals (28, 29). Recently, curcumin has been shown to confer radiosensitizing and radioprotective activities (10, 30), but the detailed mechanisms of curcumin-mediated radioprotection have not been clearly elucidated. In our study, we used curcumin treatment for 3 days pre-IR and 2 months post-IR. Mice treated with curcumin presented significant decrease in apoptotic cells and changes in both levels of inflammation as well as in long-term effect markers. Specifically, the levels of IL6 in both intestinal lysates and blood samples were significantly reduced after curcumin treatment. H&E staining of intestinal sections revealed that mice treated with curcumin presented a significantly lower number of areas of serosal fibrosis compared with the control group that showed extensive fibrotic areas on the marker site along with aggregates of lymphocytes, plasma cells, and neutrophils. So far, administration of curcumin has been shown to significantly reduce the levels of inflammatory markers and substantially reduced the fibrosis formation as a long-term effect post-IR. Taken together, these data along with the fact that curcumin is characterized by low toxicity profile, as it has been shown in phase I and II clinical trials (31), make it a potent radioprotector.

In conclusion, we developed a novel mouse model as a new tool for precise and quantitative evaluation of multiple biological markers of radiation-induced DNA damage in short segments of the intestine. Results from curcumin treatment indicated significant radioprotection in both acute and long-term effects. Thus, this model can also be used for future screens of radiation response modifiers.

Disclosure of Potential Conflicts of Interest

No potential conflicts of interest were disclosed.

Authors' Contributions

Conception and design: I.I. Verginadis, B. Bell, E. Ben-Josef, C. Koumenis
Development of methodology: I.I. Verginadis, R. Kanade, B. Bell, E. Ben-Josef, C. Koumenis
Acquisition of data (provided animals, acquired and managed patients, provided facilities, etc.): I.I. Verginadis, R. Kanade, B. Bell, S. Koduri, C. Koumenis
Analysis and interpretation of data (e.g., statistical analysis, biostatistics, computational analysis): I.I. Verginadis, R. Kanade, B. Bell, E. Ben-Josef, C. Koumenis
Writing, review, and/or revision of the manuscript: I.I. Verginadis, E. Ben-Josef, C. Koumenis

Administrative, technical, or material support (i.e., reporting or organizing data, constructing databases): I.I. Verginadis, E. Ben-Josef, C. Koumenis
Study supervision: C. Koumenis

Grant Support

This work was supported by Development funds from the Department of the Radiation Oncology, Perelman School of Medicine, University of Pennsylvania (Philadelphia, PA). I.I. Verginadis is supported by a postdoctoral fellowship from the Bodossaki Foundation (Greece).

The costs of publication of this article were defrayed in part by the payment of page charges. This article must therefore be hereby marked *advertisement* in accordance with 18 U.S.C. Section 1734 solely to indicate this fact.

Received October 6, 2016; revised November 14, 2016; accepted November 23, 2016; published OnlineFirst December 23, 2016.

References

1. Delaney G, Jacob S, Featherstone C, Barton M. The role of radiotherapy in cancer treatment: estimating optimal utilization from a review of evidence-based clinical guidelines. Cancer 2005;104:1129–37.
2. Andreyev HJ. Gastrointestinal problems after pelvic radiotherapy: the past, the present and the future. Clin Oncol (R Coll Radiol) 2007;19:790–9.
3. Mettler FAJr, Voelz GL. Major radiation exposure–what to expect and how to respond. N Engl J Med 2002;346:1554–61.
4. Hauer-Jensen M, Poulakos L, Osborne JW. Effects of accelerated fractionation on radiation injury of the small intestine: a new rat model. Int J Radiat Oncol Biol Phys 1988;14:1205–12.
5. Jagetia GC. Radioprotection and radiosensitization by curcumin. Adv Exp Med Biol 2007;595:301–20.
6. Tuttle S, Hertan L, Daurio N, Porter S, Kaushick C, Li D, et al. The chemopreventive and clinically used agent curcumin sensitizes HPV (−) but not HPV (+) HNSCC to ionizing radiation, in vitro and in a mouse orthotopic model. Cancer Biol Ther 2012;13:575–84.
7. Lao CD, Ruffin MTt, Normolle D, Heath DD, Murray SI, Bailey JM, et al. Dose escalation of a curcuminoid formulation. BMC Complement Altern Med 2006;6:10.
8. Cheng AL, Hsu CH, Lin JK, Hsu MM, Ho YF, Shen TS, et al. Phase I clinical trial of curcumin, a chemopreventive agent, in patients with high-risk or pre-malignant lesions. Anticancer Res 2001;21:2895–900.
9. Verma V. Relationship and interactions of curcumin with radiation therapy. World J Clin Oncol 2016;7:275–83.
10. Akpolat M, Kanter M, Uzal MC. Protective effects of curcumin against gamma radiation-induced ileal mucosal damage. Arch Toxicol 2009; 83:609–17.
11. Leibowitz BJ, Wei L, Zhang L, Ping X, Epperly M, Greenberger J, et al. Ionizing irradiation induces acute haematopoietic syndrome and gastrointestinal syndrome independently in mice. Nat Commun 2014; 5:3494.
12. Leibowitz BJ, Qiu W, Liu H, Cheng T, Zhang L, Yu J. Uncoupling p53 functions in radiation-induced intestinal damage via PUMA and p21. Mol Cancer Res 2011;9:616–25.
13. Salic A, Mitchison TJ. A chemical method for fast and sensitive detection of DNA synthesis *invivo*. Proc Natl Acad Sci U S A 2008;105:2415–20.
14. Garg S, Boerma M, Wang J, Fu Q, Loose DS, Kumar KS, et al. Influence of sublethal total-body irradiation on immune cell populations in the intestinal mucosa. Radiat Res 2010;173:469–78.
15. Hauer-Jensen M, Wang J, Denham JW. Bowel injury: current and evolving management strategies. Semin Radiat Oncol 2003;13:357–71.
16. Fajardo LF. The pathology of ionizing radiation as defined by morphologic patterns. Acta Oncol 2005;44:13–22.
17. Martin M, Lefaix J, Delanian S. TGF-beta1 and radiation fibrosis: a master switch and a specific therapeutic target? Int J Radiat Oncol Biol Phys 2000;47:277–90.
18. Elhammali A, Patel M, Weinberg B, Verma V, Liu J, Olsen JR, et al. Late gastrointestinal tissue effects after hypofractionated radiation therapy of the pancreas. Radiat Oncol 2015;10:186.
19. Murphy JD, Christman-Skieller C, Kim J, Dieterich S, Chang DT, Koong AC. A dosimetric model of duodenal toxicity after stereotactic body radiotherapy for pancreatic cancer. Int J Radiat Oncol Biol Phys 2010;78:1420–6.
20. Ben-Josef E, Schipper M, Francis IR, Hadley S, Ten-Haken R, Lawrence T, et al. A phase I/II trial of intensity modulated radiation (IMRT) dose escalation with concurrent fixed-dose rate gemcitabine (FDR-G) in patients with unresectable pancreatic cancer. Int J Radiat Oncol Biol Phys 2012; 84:1166–71.
21. Hauer Jensen M, Sauer T, Reitan JB, Nygaard K. Late radiation enteropathy following split-dose irradiation of rat small intestine. Acta Radiol Oncol 1986;25:203–6.
22. Peck JW, Gibbs FAJr. Assay of premorbid murine jejunal fibrosis based on mechanical changes after X irradiation and hyperthermia. Radiat Res 1987;112:525–43.
23. De Both NJ, Vermey M. Epithelial regeneration of transposed intestine after high doses of X-irradiation. Int J Radiat Biol Relat Stud Phys Chem Med 1976;29:17–26.
24. Potten CS. Radiation, the ideal cytotoxic agent for studying the cell biology of tissues such as the small intestine. Radiat Res 2004;161:123–36.
25. Denham JW, Hauer-Jensen M, Peters LJ. Is it time for a new formalism to categorize normal tissue radiation injury? Int J Radiat Oncol Biol Phys 2001;50:1105–6.
26. Carr KE. Effects of radiation damage on intestinal morphology. Int Rev Cytol 2001;208:1–119.
27. Kavanagh BD, Pan CC, Dawson LA, Das SK, Li XA, Ten Haken RK, et al. Radiation dose-volume effects in the stomach and small bowel. Int J Radiat Oncol Biol Phys 2010;76:S101–7.
28. Kouvaris JR, Kouloulias VE, Vlahos LJ. Amifostine: the first selective-target and broad-spectrum radioprotector. Oncologist 2007;12:738–47.
29. Vujaskovic Z, Feng QF, Rabbani ZN, Samulski TV, Anscher MS, Brizel DM. Assessment of the protective effect of amifostine on radiation-induced pulmonary toxicity. Exp Lung Res 2002;28:577–90.
30. Javvadi P, Hertan L, Kosoff R, Datta T, Kolev J, Mick R, et al. Thioredoxin reductase-1 mediates curcumin-induced radiosensitization of squamous carcinoma cells. Cancer Res 2010;70:1941–50.
31. Goel A, Kunnumakkara AB, Aggarwal BB. Curcumin as "Curecumin": from kitchen to clinic. Biochem Pharmacol 2008;75:787–809.